

Natural large-scale structures in the axisymmetric mixing layer

By K. B. M. Q. ZAMAN† AND A. K. M. F. HUSSAIN

Mechanical Engineering Department, University of Houston, Texas 77004

(Received 19 July 1982 and in revised form 17 May 1983)

This paper summarizes results of our investigations on: optimization of conditional sampling technique for eduction of naturally occurring large-scale structures in an axisymmetric mixing layer, comparison of the natural structure with that induced via controlled excitation, and the sensitivity of the educed structure to the excitation amplitude and of the natural coherent structure to Reynolds number and initial condition. Measurements include sectional-plane contours of various structure properties; however, coherent vorticity is the principal measure used in these considerations. All plausible alternative triggering criteria, based on reference velocity signals from fixed probes, were considered in order to arrive at the best practical eduction technique. It is shown that the simple criterion of triggering on the positive peaks of the longitudinal velocity signal derived from the high-speed edge of the mixing layer results in the optimum eduction. The characteristics of the natural structures, educed by the optimum detection criterion, are found to be independent of Re_D over the measurement range 5.5×10^4 – 8×10^5 . A mild dependence on the initial condition (viz laminar *vs.* turbulent) is observed, the structures being more disorganized for the initially laminar boundary-layer case. The educed natural structures agree well with those induced by controlled sinusoidal excitation at low excitation levels; higher levels, however, produce considerably stronger structures.

1. Introduction

A number of large-scale structure studies have been carried out in the circular jet, especially in the near field. Although this flow, i.e. the axisymmetric shear layer, might appear to be a simple one, it is considerably more complicated than a plane shear layer, because this flow is characterized by two lengthscales: the initial shear-layer characteristic thickness (e.g. the momentum thickness θ) and the jet diameter D . The initially rolled-up vortical structures which scale on θ (Michalke 1965), anticascade (through amalgamations) and grow in size with x . At a distance x comparable to D , the diameter becomes the controlling lengthscale. Thus the ratio D/θ is an additional parameter controlling the characteristics and evolution of the large-scale structures in the axisymmetric mixing layer. The development of azimuthal lobes (Widnall 1975) and the occurrence of higher-order instability modes (Mattingly & Chang 1974; Armstrong, Michalke & Fuchs 1977; Moore 1977; Petersen 1978; Drubka & Nagib 1981) further add to the complexity of the coherent structure evolution in this flow.

While the details of the large-scale structures in the self-preserving region of a circular jet are yet to be conclusively documented, the formation and subsequent

† Present address: NASA-Langley Research Center, Hampton, VA 23665.

development of the structures in the initial region of the jet have been studied by many (e.g. Crow & Champagne 1971; Browand & Laufer 1975; Kibens 1980; Davies & Baxter 1978; Bruun 1977; Yule 1978). One of the techniques frequently employed in these studies is controlled excitation, which triggers the formation of the structures at regular intervals and removes much of the jitter in the structure parameters, so that eduction of the structures is facilitated via phase-locked measurements. Controlled excitation was employed by us to study vortex pairing (Zaman & Hussain 1980) as well as the 'preferred mode' structure (Hussain & Zaman 1981, hereinafter referred to as I). In I, jets at different Reynolds numbers and initial conditions were studied under excitation at the Strouhal number $St_D = 0.30$, which corresponds to the passage frequency of the dominant structure near the end of the potential core, and the characteristics of the induced coherent structure were documented. It should be emphasized that controlled excitation enabled us to educe the structure in greater detail than is likely to be possible in the unexcited case. However, the obvious question as to how well the artificially induced structures represent the naturally occurring ones has remained unanswered.

Attempts to use conditional-sampling techniques for eduction of the naturally occurring large-scale structure in free shear flows have been limited. Most relevant to the present study are the works of Browand & Weidman (1976), Bruun (1977, 1979), and Yule (1978). Browand & Weidman (1976) made measurements in a two-stream plane (water) shear layer at a low Reynolds number. They used two reference probes, one on the high-speed side and the other on the low-speed side, to trigger data sampling by a third sensor. By using the peaks and troughs in the two reference signals at selected phase differences as triggering conditions, they educed the structures at two distinct stages of interaction. Bruun (1977) and Yule (1978) made conditional measurements in the near field of the round jet. While Bruun worked at $Re_D = 10^4$, Yule used a moderately higher Re_D of 4.3×10^4 ; presumably, the exit boundary layer was laminar in each case. They triggered the eduction on the peaks of a reference \bar{u} -signal (a.c. coupled), obtained from the high-speed side; Bruun used the positive peaks above 2σ and Yule used the negative peaks below -2.8σ , σ being the r.m.s. of the reference signal. Bruun obtained ensemble-averaged longitudinal velocity traces at different positions in the flow, and qualitatively inferred the large-scale structure signature from composite plots of these traces. Yule made limited measurements with an X-wire to obtain the ensemble-averaged streamline pattern associated with the large-scale structure. Bruun (1979) extended his technique (Bruun 1977) to obtain ensemble-averaged velocity traces for a much higher Re_D (2×10^5) and observed the traces to vary considerably from those at lower Re_D . Thus, not only the eduction technique itself has remained highly subjective and ambiguous, but also the effects of variations in the Reynolds number and the initial condition on the eduction technique and on the coherent structure properties have remained unexplored.

Past experimental evidence raised some doubts about Reynolds-number similarity in axisymmetric mixing layers. Crow & Champagne (1971) observed changes in the organized motions in a jet with the Reynolds number. While the time-average measures did not appear to directly depend on Re_D (Hussain & Zedan 1978), flow visualization indicated that the organization of the large structures decreased with increasing Re_D (Clark 1979). In I, the structure details under excitation also showed a mild Re_D dependence. Effects of the initial condition have been observed to persist in the axisymmetric mixing layer, even up to the end of the potential core (Bradshaw 1966). Thus the effects of the Reynolds number and the initial condition

even on the time-average measures of the axisymmetric mixing layer have remained unresolved. Indeed, at the beginning of the present study, there were doubts as to whether the large-scale structures could be educed at very high Re_D and for the initially fully turbulent case.

The present study was carried out in two phases. The first phase involved evaluation of the conditional-sampling technique and determination of the optimum technique. Several questions could be raised regarding the choice of the sampling criteria and plausible alternatives in the technique. For example, when using the peaks of a reference velocity signal, what is the optimum threshold level? How would the structure educed by the positive peaks compare with that educed by the negative peaks? Would the peaks of a \tilde{v} -signal, or some combined criteria based on \tilde{u} and \tilde{v} work better for the eduction? What effect would the exact location of the trigger probe have on the educed structures? Could a joint criterion based on the peaks and troughs of two reference signals from the high- and low-speed sides of the shear layer – as used by Browand & Weidman (1976) – work in the much higher Reynolds number axisymmetric mixing layer? (The Reynolds number based on the maximum slope thickness for the flow discussed in §3 was about 50000, as opposed to 300 in Browand & Weidman's study.) These questions were addressed in the first phase of this study.

The second phase involved the application of the optimum eduction technique to document the detailed properties of the natural coherent structures and compare them with artificially induced structures. These were done for different Reynolds numbers and initial conditions. These comparisons allowed us to determine: if the artificially induced structures differed from the natural structures, the extent to which the structure properties were sensitive to the excitation amplitude, whether the chosen eduction scheme worked well at very high Re_D , whether Reynolds-number similarity held for the large-scale structures, and the extent to which the structures were affected by the initial condition.

2. Experimental procedures

The comparative evaluation of the conditional-sampling technique was carried out in a 7.6 cm circular air jet at a Reynolds number $Re_D = 110\,000$. The nozzle boundary layer was tripped with a sand-paper ring located 4 cm upstream from the exit plane. The efflux boundary layer was fully turbulent as diagnosed by the \tilde{u} -spectrum, and confirmed by the profiles of the longitudinal mean and r.m.s. velocities (U , u'). The mean velocity profile had a shape factor of 1.4 and had the characteristic logarithmic and wake regions in the universal (U^+ , y^+)-coordinates with the 'wake strength' agreeing with that expected at the corresponding $Re_\theta (= U_e \theta / \nu)$ value of the exit boundary layer. The fluctuation intensity u'/U_r was about 2.4, and peaked at $y^+ \sim 15$. The spectrum was broadband without any spikes. The jet emerged with a top-hat mean-velocity profile and the freestream turbulence intensity at the exit plane was 0.2%. Details of this jet facility were described by Zaman & Hussain (1980). For studying the Re_D and initial-condition dependence, data were also acquired in a second jet facility having a 76 cm diameter settling chamber with similar flow quality at the exit (of a 27 cm nozzle) as in the first one, and in a third, even larger (but noisier), jet facility driven by an axial fan and discharging through a 30 cm or a 15 cm nozzle.

Most of the data presented in this paper pertain to the downstream station of $x/D = 3$. Velocity signals from a measurement X-wire probe and two reference probes were recorded by an on-line computer (HP2100S) onto a digital magnetic tape. Data

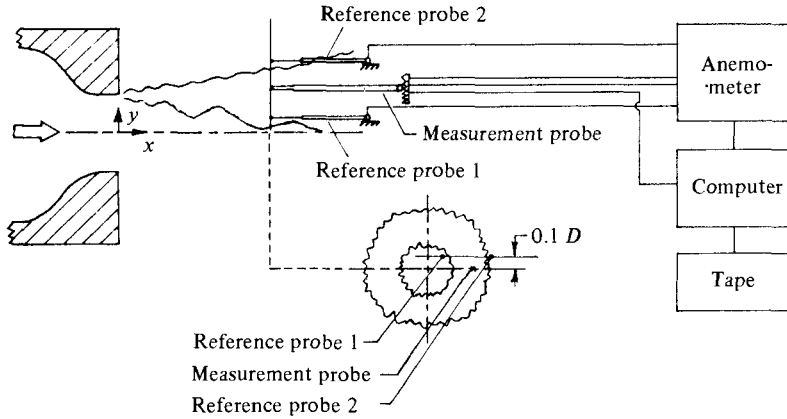


FIGURE 1. Schematic of the probe positions in the flow and instrumentation.

were acquired for different radial positions (y) of the X-wire while the single-wire reference probe(s) were held fixed. In some of the measurements, only one X-wire reference probe was used on the high-speed side. The reference probe(s) were placed at the same axial station as that of the measurement probe but were displaced in the azimuthal direction by $0.1D$, so that the X-wire could be moved without interfering with the reference wire. The relative probe positions in the flow are schematically shown in figure 1. Data were obtained by standard linearized hot-wire (DISA) anemometers. An analog (DISA) turbulence processor was used to obtain the longitudinal (\tilde{u}) and radial (\tilde{v}) velocity components from the X-wire signals. A 500-line spectrum analyser (Spectrascope SD335) was used to obtain \tilde{u} -spectra.

At a particular y -station, four 'simultaneous' velocity signals were recorded; these were the reference signals from the high-speed side (\tilde{u}_{r1}) and the zero-speed side (\tilde{u}_{r2}), and the \tilde{u} - and \tilde{v} -velocities. When an X-wire was used as the reference probe (on the high-speed side), \tilde{v}_{r1} replaced \tilde{u}_{r2} . In all cases, the two reference signals were bandpass-filtered between 1 Hz and $8f_m$, where f_m corresponds to St_D ($=f_m D/U_e$) = 0.45 and is the frequency of the peak in the \tilde{u} -spectrum measured on the jet centreline at $x/D = 3$. The four 'simultaneous' signals were sampled at a rate such that 64 adjacent time steps approximately spanned twice the passage interval of the structure. Time-series data of the four signals, in batches of 3000 each, were recorded on a digital tape for a total of 15 y -stations, the measurement probe having been traversed via automated and remote computer control. The number of sample functions recorded for each signal at each station was 110. The time-series data were later analysed by the laboratory computer; the procedures are described along with the respective results.

3. Considerations in the eduction

The spectral evolution on the jet axis is shown in figure 2(a) for $0 < x/D < 8$. Note that the shear-layer activity is 'felt' on the jet centreline only for $x/D \lesssim 1.5$ and that the structure 'footprint' is lost for $x/D \gtrsim 8$. The frequency of the spectral peak shows a gradual decrease from about $St_D \approx 0.55$ at $x/D = 2$ to about 0.30 at $x/D = 5$. Measurements at a few other values of Re_D over the range $5 \times 10^4 \gtrsim Re_D \gtrsim 10^6$ in different facilities showed essentially the same trend as in figure 2(a) (see also §4.1).

A gradual decrease of the spectral peak frequency with increasing x was also

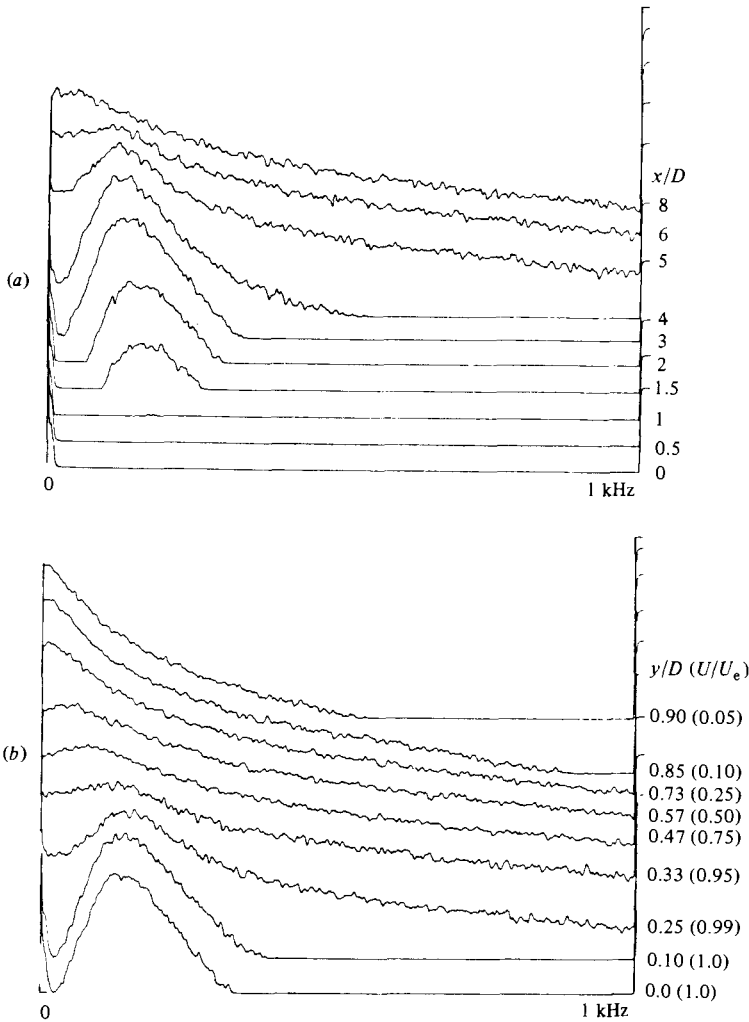


FIGURE 2. Spectra of \tilde{u} in the 7.6 cm (tripped) jet at $Re_D = 110000$: (a) for different axial stations on the jet centreline; (b) for different transverse locations at $x/D = 3$.

observed in jets with initially laminar boundary layers by previous investigators (e.g. Ko & Davies 1971; Browand & Laufer 1975; Davies & Baxter 1978). Browand & Laufer (1975) hypothesized that the organized structures in the circular jet achieve independence from the initial rolled-up vortex rings (formed at relatively higher frequencies), through a number of stages of pairing and attain the 'terminal Strouhal number' at the end of the potential core. While this argument is plausible for initially laminar boundary-layer cases, especially when the two frequencies are in appropriate ratios (Kibens 1980), the mechanism for the 'roll-up' in the initially turbulent boundary-layer case remains to be explained. Since, in the latter case, the peak in the \tilde{u} -spectra occurs at a constant St_D for a certain x/D but for a wide Re_D range (and for a wide range of D/θ), it appears that this unique 'roll-up' frequency and the corresponding large-scale structure are characteristic of the axisymmetric configuration.

Figure 2(b) shows the \tilde{u} -spectra at $x/D = 3$ for different y/D ; the corresponding

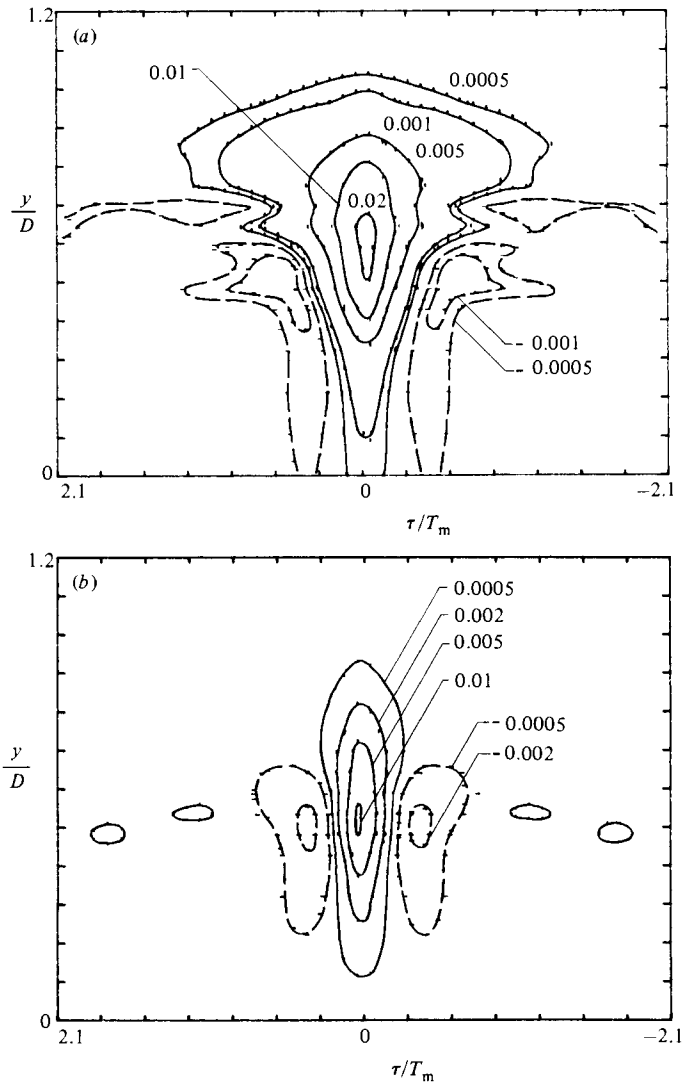


FIGURE 3(a, b). For caption see facing page.

mean velocities are also indicated. The traces in the potential core (i.e. at $y/D = 0, 0.1$ and 0.25) show broadband but distinct peaks; there appears to be a slight increase in the frequency as the edge of the shear layer is approached from the jet centerline (see also Lau, Fisher & Fuchs 1972). As y is increased farther, energy accumulates in lower frequency ranges. The spectra on the low-speed side in figure 2(b) and at y -stations farther away (for $U/U_e \gtrsim 0.01$), do not show any clear peak. The essential absence of any 'spectral footprint' on the zero-speed side contrasts the suggestion of Lau *et al.* (1972). But it is not inconsistent with Yule's (1978) claim that the structure is organized on the high-speed side but quite smeared on the outer side (even though instantaneous smoke pictures do not show any difference between the inner and the outer boundaries - Clark 1979). It should be remembered that the zero-speed-side hot-wire measurements are significantly affected by flow reversal (Antonia, Satyaprakash & Hussain 1980) as well as radial ejection of the core fluid.

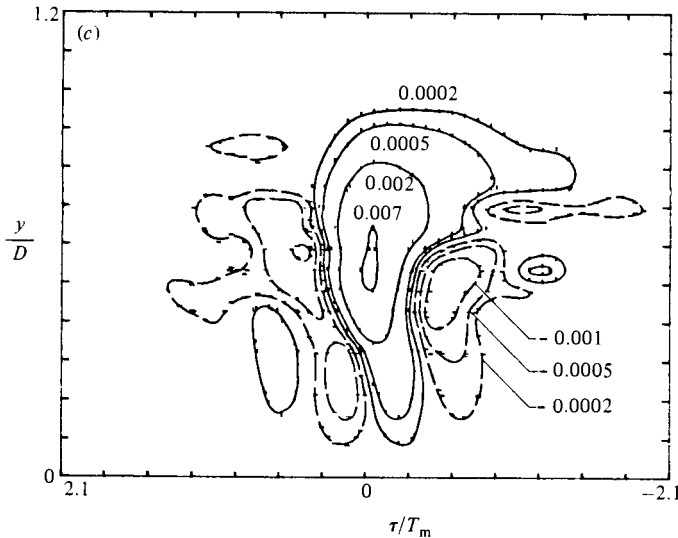


FIGURE 3. Contours of correlations of the \tilde{u} - and \tilde{v} -velocity components for $x/D = 3$; T_m is such that $D/(U_e T_m) = 0.45$: (a) $\overline{u\tilde{u}(\tau)}/U_e^2$; (b) $\overline{v\tilde{v}(\tau)}/U_e^2$; (c) $\overline{u\tilde{v}(\tau)}/U_e^2$.

The quasi-periodicity in the signal at $x/D = 3$ is further demonstrated in figure 3. The variations of the correlations $\overline{u\tilde{u}(\tau)}$, $\overline{v\tilde{v}(\tau)}$, and $\overline{u\tilde{v}(\tau)}$ across the mixing layer are presented as contour maps in figures 3(a, b, c), respectively. These correlations, between the fluctuating components of the velocities, are non-dimensionalized by U_e^2 so that the contours not only indicate the spatial and temporal coherence but also comparative distributions of the three stresses. Figure 3(a) shows that the period of the oscillating $\overline{u\tilde{u}(\tau)}$ remains approximately constant in the potential core and the periodicity is progressively lost as the middle of the shear layer is approached. Note that the periodicity in $\overline{v\tilde{v}(\tau)}$ persists well inside the shear-layer region. The \tilde{v} -signal, which may thus appear more attractive as a reference signal in the eduction of the structures, suffers from other constraints (see later). $\overline{v\tilde{v}(\tau)}$ contours cease to exist as the jet centreline is approached because v is zero on the centerline. This is not so with $\overline{u\tilde{u}(\tau)}$, as the flow must accelerate on the centreline as it passes through the toroidal structure. Note that the maximum level of $\overline{v\tilde{v}(\tau)}$ is about half that of $\overline{u\tilde{u}(\tau)}$. Note also that $\overline{u\tilde{v}(\tau)}$ is antisymmetric only in the potential core (up to about $y/D = 0.3$), but has a maximum at $\tau = 0$ within the shear layer, as to be expected. The period T_m in the oscillation of all three quantities, easily measurable only on the high-speed side, is found to be the same and corresponds to the Strouhal number $D/T_m U_e = 0.45$.

Reference velocity signals from stationary probes were used to educe the large-scale structure characteristics in the unexcited axisymmetric mixing layer. Figure 4 shows typical samples of simultaneous velocity signals in the following sequence: reference signal \tilde{u}_{r1} from the high-speed side, reference signal \tilde{u}_{r2} from the zero-speed side, and the \tilde{u} - and \tilde{v} -signals from the X-wire probe at $y/D = 0.21$. All the signals, at $x/D = 3$ and for the probe configuration shown in figure 1, have identical horizontal scales but arbitrary vertical scales. In figure 4, \tilde{u}_{r1} shows large negative spikes while \tilde{u}_{r2} shows large positive spikes. It is believed that the negative spikes represent instants when low-momentum fluid is ingested and swept past the probe on the high-speed side, and the positive spikes when the high-momentum fluid is transported

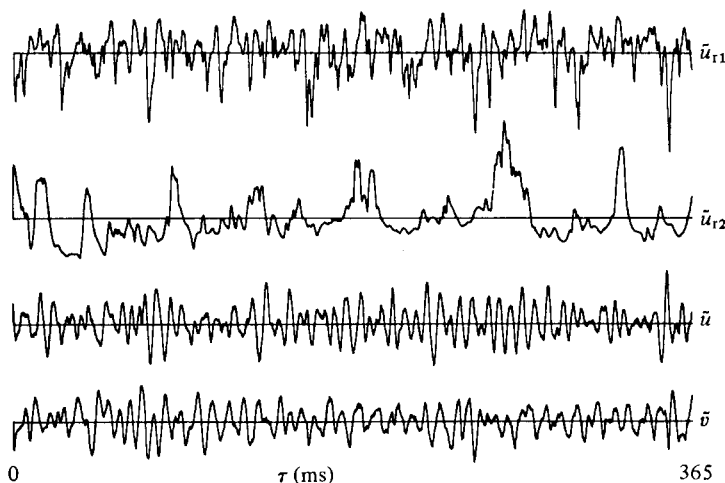


FIGURE 4. Simultaneous time traces of the reference signals \tilde{u}_{r1} (at $y/D = 0.33$; $U/U_e \approx 0.95$) and \tilde{u}_{r2} (at $y/D = 0.85$; $U/U_e \approx 0.10$), and the \tilde{u} - and \tilde{v} -signals (measured at $y/D = 0.21$). Horizontal scales are the same but vertical scales are arbitrary.

outwards and swept past the probe on the zero-speed side (see also Bruun 1977; Yule 1978; Lau 1979). Lau observed that the frequency of the negative spikes was about 3 times that of the positive spikes, which led him to hypothesize a two-street coherent structure model for the axisymmetric jet. Studies via flow-visualization and hot-wire measurements in a natural jet (Clark 1979), as well as in jets under artificial excitation, did not bear out this hypothesis.

Examination of a large number of traces of \tilde{u}_{r1} and \tilde{u}_{r2} as in figure 4 showed that the spacings of the spikes vary widely. The typical time lapses between the negative spikes of \tilde{u}_{r1} (as well as between the positive spikes of \tilde{u}_{r2}) are found to be far larger than the 7.5 ms period corresponding to the peak in the \tilde{u} -spectrum. Assuming these spikes to be associated with large-scale structures, it appears that either the structures are occasionally large and energetic enough to produce the infrequent spikes or they pass nearby the sensor(s) only occasionally. The correspondence between the negative spikes in \tilde{u}_{r1} and the positive spikes in \tilde{u}_{r2} is an important question to be addressed later; but, first, we will examine conditional measurements using \tilde{u}_{r1} as the only reference signal.

3.1. Eduction with the high-speed-side reference signal

The negative peaks of \tilde{u}_{r1} were first used as the trigger criterion. The instants of occurrence of the peaks below a set threshold were used as trigger (i.e. $\tau = 0$) to accept sample functions $\tilde{u}(t)$ and $\tilde{v}(t)$; for trigger, the peak locations rather than the threshold locations were considered better by Bruun (1977). Thus the triggers are the reference points for alignment of successive structure signatures. This straightforward alignment does not involve any time-shifting, and is thus different from the 'overall alignment' used by Zilberman, Wygnanski & Kaplan (1977) and Sokolov *et al.* (1980). The latter studies involved relative shifting of data records via maximization of cross-correlation so that alignment was based on overall structure signature rather than on a front or a peak. The 'overall alignment' has the disadvantage of taking long computer time as well as diluting the peak. The present alignment would produce less smearing in the peak value but more smearing in regions far from the triggering

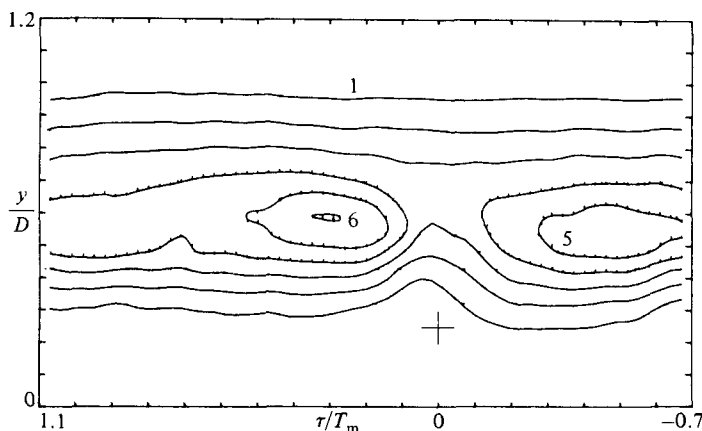


FIGURE 5. Ω_z/f_m contours educed by the $\tilde{u}_{r1} < -2\sigma$ criterion.

probe. For the present study, the peak coherent vorticity within a structure was considered more crucial than the details of its outer boundary.

Each of the accepted 'data bursts' of $\tilde{u}(t)$ and $\tilde{v}(t)$ consisted of 64 data points with 31 points preceding the trigger and 32 points following. Ensemble averages $\langle u \rangle$ and $\langle v \rangle$ of the accepted realizations were further processed to obtain the total coherent azimuthal vorticity $\Omega_z (= -(1/0.5U_e) \partial \langle v \rangle / \partial t - \partial \langle u \rangle / \partial y)$ distribution in a (τ, y) -plane; $\langle u \rangle$ and $\langle v \rangle$ represents the total coherent components of the velocities. Ω_z was non-dimensionalized by the frequency f_m (corresponding to the peak in the spectrum) such that $f_m D/U_e = 0.45$. The time axis is non-dimensionalized by the corresponding period $T_m (= 1/f_m)$. Note that, in computing Ω_z , the Taylor hypothesis has been invoked using a convection velocity of $0.5U_e$; the validity of the hypothesis for eduction of non-interacting large-scale structures was demonstrated by Zaman & Hussain (1981).

3.1.1. Structure identification

The vorticity Ω_z distribution educed by the criterion of $\tilde{u}_{r1} < -2\sigma$ is shown in figure 5. The reference probe providing the \tilde{u}_{r1} signal was placed at $y/D = 0.25$ ($U/U_e = 0.99$). The trigger locations in this and the following figures are identified by the + sign. Yule (1978) had educed the streamline pattern in the mixing layer of a 5.08 cm jet at $Re_D = 43000$, also triggering on the negative spikes of a reference u -signal obtained from the high-speed side. The longitudinal spacing of the structures and their transverse locations in figure 5 agree well with those found by Yule. However, compared to the streamline pattern (i.e. the velocity vector field) obtained by Yule, the educed structures in figure 5 are clearer, and are also quantified via the contour levels.

A number of properties can be used to characterize the coherent structures. These may include: contours of ensemble-averaged velocity components, streamlines, coherent vorticity, coherent and incoherent Reynolds stresses, turbulence intensities, strain rate, and productions, etc. Experience with these properties in a number of flows suggests that coherent vorticity is by far the most useful single property. It not only gives the boundary of a structure (hence shape and size) but also its strength (denoted by peak vorticity). In particular, unlike streamlines and some other properties, Ω_z is independent of Galilean transformation and hence is preferable

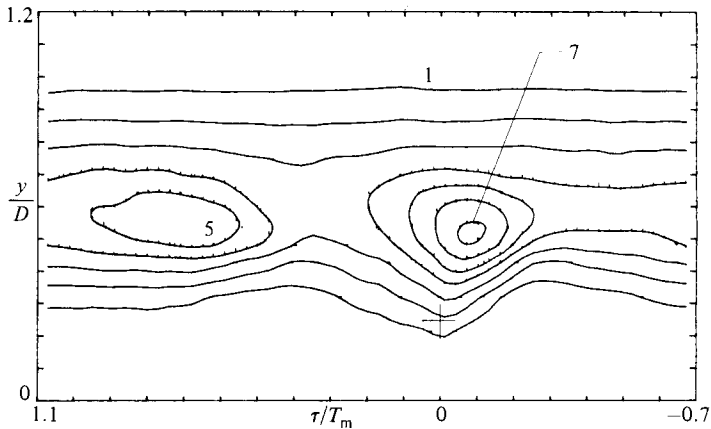


FIGURE 6. Ω_z/f_m contours educed by the $\tilde{u}_{r1} > 2\sigma$ criterion.

for structure identification. Thus Ω_z has been used here as the primary measure for evaluation of the eduction technique. Some of the other properties will be briefly discussed in §4.3.

3.1.2. Smearing effect and comparison with structure under excitation

Figure 6 shows the Ω_z distribution from the same data set as in figure 5 but using the positive peaks in \tilde{u}_{r1} ($> 2\sigma$) for trigger. Clearly, this criterion results in eduction of the structure having a higher peak vorticity and, consequently, larger number of closed contours. Since a larger core cross-section and a higher peak vorticity represent better approximation of the most energetic structure, the positive-peak criterion (figure 6) is considered superior to the negative-peak criterion (figure 5).

Lesser smearing occurs with the positive-peak criterion because the educed structure centre at the instant of trigger is physically located at the same x as the reference probe. On the other hand, when triggering on the negative peak of \tilde{u}_{r1} , the reference wire is located halfway between two structures. Thus, in the latter case, the structure is educed when centred away from the trigger. The farther away is the measurement point from the trigger the more is the phase jitter, resulting in smeared-out educed structures. This is why use of the positive peaks produces less smearing.

In choosing the best criterion for the conditional sampling, the educed structures are compared on the following bases: (i) the number of closed contours and the peak level of Ω_z ; (ii) the streamwise and transverse extents of the educed structure; and (iii) comparison with the educed structure when induced by a small-amplitude excitation approximately at the frequency f_m . For the last criterion, Ω_z contours were obtained in the present flow subjected to controlled excitation at a frequency of 144 Hz; note that 144 Hz corresponded to $St_D = 0.49$ and was the excitation frequency available nearest to f_m , providing a uniform excitation of desired amplitude at the jet exit plane. The excitation characteristics are documented by \hat{u} -spectra in figure 7. The upper and middle traces represent the flow with and without the excitation, at $x/D = 3$ on the jet axis. The bottom trace is for the excitation case at the jet exit centre. The excitation, provided by means of a loudspeaker attached to the side of the settling chamber, was of an amplitude of $u'_{re}/U_e = 0.1\%$, where u'_{re} is the r.m.s. of the fundamental measured at the jet-exit centre. The spectral spike corresponding to u'_{re} is marked in the bottom trace. Note that the other prominent

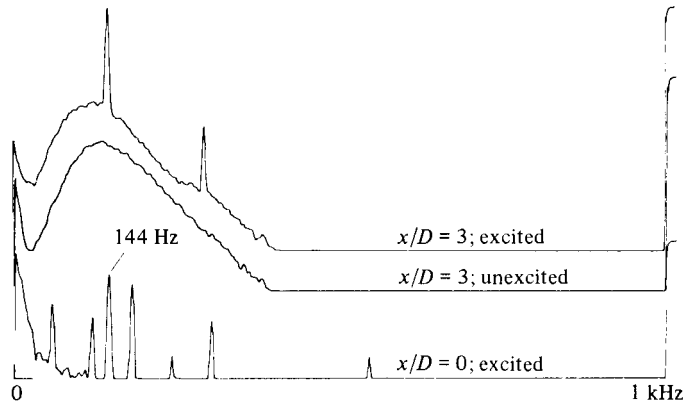


FIGURE 7. \tilde{u} -spectra traces for the excitation case; $f_p = 144$ Hz, $u'_{te}/U_e = 0.1\%$. Measurements on the centreline of the 7.6 cm (tripped) jet at $Re_D = 110000$.

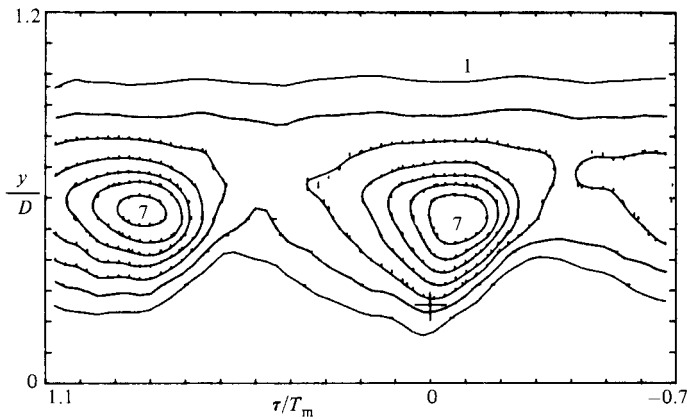


FIGURE 8. Ω_z/f_m contours educed by the $\tilde{u}_{r1} > 2\sigma$ criterion for the flow corresponding to figure 7.

spikes in this trace are at the line frequency (60 Hz) and its harmonics, principally due to linearizer noise, and hence are of no significance to the flow. It should be noted that the spike at 144 Hz in the top trace (with logarithmic ordinate) is quite large and indicates a strong organization of the large-scale structures.

For the excited flow, the Ω_z contours obtained with the $\tilde{u}_{r1} > 2\sigma$ criterion (resulting in almost 100% acceptance of the data records) are shown in figure 8. As the detection scheme is progressively refined, the educed natural structure should approach this structure until the best scheme is developed. This, of course, assumes that the effect of the excitation is only to organize the natural structures (see §4.2 and also I). Comparison of figures 6 and 8 shows that the $\tilde{u}_{r1} > 2\sigma$ criterion educed the dominant natural structure quite successfully. However, some unavoidable smearing in the natural case resulted in a somewhat smaller core cross-section in figure 6. The smearing effect increases with increasing time separation between measurement and trigger; for example, compare the structure on the left in figure 6 with that in figure 8. Note that the repeated structure on the left in figure 8 is almost identical with the one near the trigger, confirming periodic occurrence of the structures under the small-amplitude excitation.

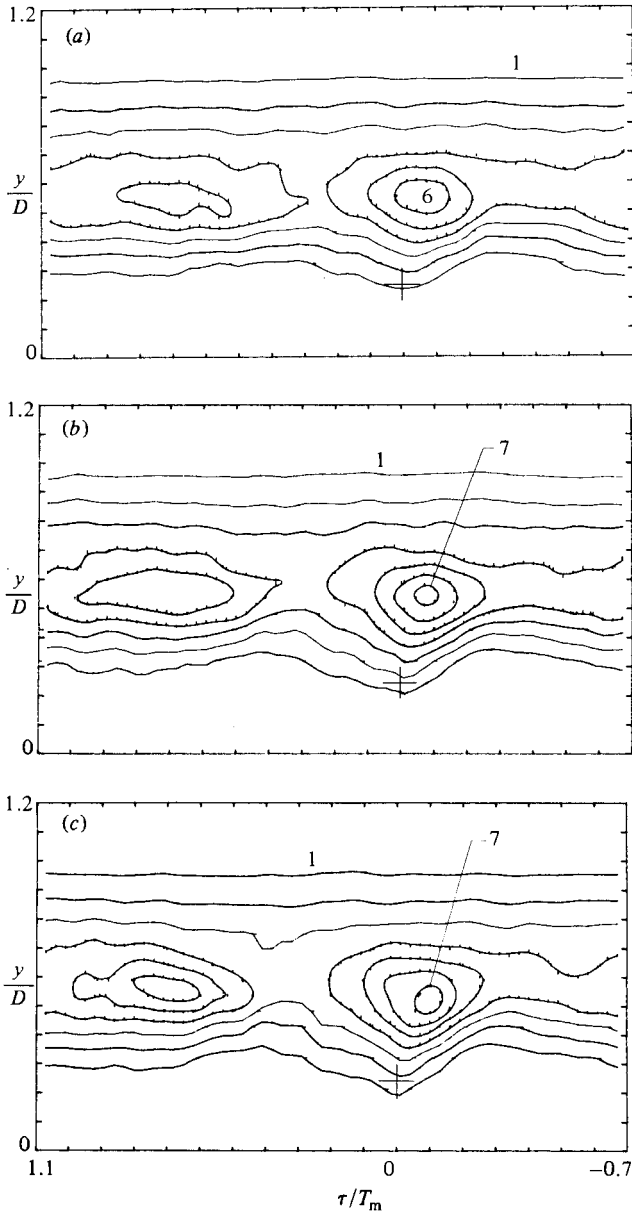


FIGURE 9(a-c). For caption see facing page.

3.1.3. Effects of the threshold level

In using an amplitude-dependent trigger condition, one must consider the selection of the optimum threshold level. For a given data volume, a threshold above a certain level will accept too few realizations producing large scatter in the ensemble averages; so convergence will require a prohibitively large experiment time. On the other hand, if the threshold is too low, acceptance of dissimilar structures will result in excessive smearing. This effect is illustrated in figures 9(a-e), where Ω_2 contours, obtained from the same data set as in figure 6, are shown for (\tilde{u}_{r1}) threshold levels of 0.5σ , 1.5σ ,

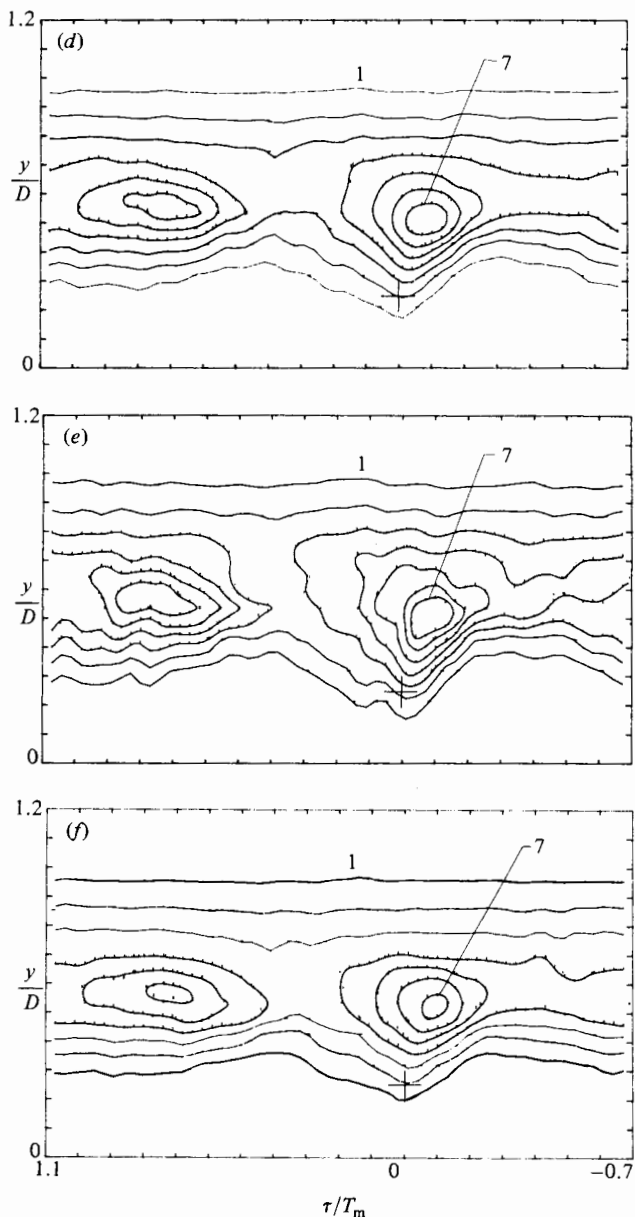


FIGURE 9. Ω_z/f_m contours educed by the $\tilde{u}_{r1} > A\sigma$ criterion. Values of A are (a) 0.5, (b) 1.5, (c) 2.0, (d) 2.5, (e) 3.0. (f) shows Ω_z/f_m contours educed by the 'window' criterion $2\sigma < \tilde{u}_{r1} < 2.4\sigma$.

2σ , 2.5σ and 3σ respectively. For proper comparison, the same ensemble size of 400 was used for all the cases, except for the 3σ case, for which the recorded data produced an ensemble size of about 75. If the entire data volume (of 3.3×10^5 data per signal per station) were used, the ensemble sizes for the 0.5σ , σ , 1.5σ , 2σ and 2.5σ threshold criteria would be about 9000, 7500, 4000, 1500 and 450 respectively. (Note that the ensemble size was 1500 in figure 6.)

Note that for the threshold of 0.5σ (and also of σ , for which data are not shown to conserve space), the $\Omega_z = 7$ contour is absent; the area enclosed by this contour increases as the threshold is increased. In figure 9(e), the accepted number of

realizations being too small, large scatter appears in the data, as to be expected. An essentially similar behaviour was observed in the Ω_z contours (not shown) obtained by varying the threshold for the negative peaks in \tilde{u}_{r1} . These contours are similar to figure 5, and the peak of Ω_z/f_m on either left or right of the trigger did not reach a value of 7, even at the threshold of -3.5σ .

Thus a higher threshold yields better education. However, improvements at threshold levels above $\tilde{u}_{r1} = 2\sigma$ are not significant. Furthermore, to obtain smooth contours with larger thresholds, one requires excessively large experiment time. As a compromise, we conclude that the $\tilde{u}_{r1} > 2\sigma$ threshold criterion yields the optimum result.

3.1.4. Effect of a trigger-level window

One would expect an improved education if a window is used for accepting the reference signal peaks rather than using only a discriminating threshold, i.e. if only structures corresponding to the peaks falling within a narrow window are ensemble-averaged. This was done for \tilde{u}_{r1} peaks falling in the window $A\sigma < \tilde{u}_{r1} < 1.2A\sigma$; education was done for $A = 0.5, 1, 1.5, 2, 2.5$ and 3. For brevity, only the one obtained with $A = 2$ is shown in figure 9(f); the ensemble size for these data was kept at 400. It was found that use of the window at lower threshold levels resulted in more smearing. For example, $A = 0.5$ resulted in a structure (not shown) much more smeared compared to the structure in figure 9(a). This is to be expected because stronger structures ought to produce larger peaks in \tilde{u}_{r1} , while all structures associated with peaks larger than 0.5σ were ensemble-averaged in figure 9(a). However, as the threshold level is increased, the difference between the contour patterns obtained with and without window becomes less. For the threshold of 2σ , there is hardly any detectable difference, as is evident from comparison of figures 9(c) and (f). Thus the improvement in the education by setting a window at the higher thresholds is found to be marginal, and the window criterion will not be considered any further.

3.2. Further considerations

3.2.1. Use of \tilde{v} -signal as reference

The structures educed with the \tilde{v}_{r1} signal are shown in figures 10(a, b) for -2σ and $+2\sigma$ thresholds respectively. The reference (X-wire) probe for these data was placed at $y/D = 0.25$. Note that, since $\tau = 0$ is the trigger location, \tilde{v} is expected to have a positive or negative peak at $\tau = 0$ according to whether the positive or negative threshold criterion is used. This is borne out by the locations of the structures relative to the trigger in figures 10(a, b) and when the induced velocity (\tilde{v}) of the structures is considered. Comparison with figure 6 indicates that \tilde{v}_{r1} is not better than \tilde{u}_{r1} for the education. Since both positive and negative \tilde{v} -peaks occur away from the structure centre, use of either as trigger results in more smearing in the educed structure, as compared with the use of the positive peaks of \tilde{u}_{r1} .

3.2.2. Effect of reference-probe location

While the structure educed with \tilde{u}_{r1} from $y/D = 0.25$ has been shown in figure 6, those educed with \tilde{u}_{r1} from $y/D = 0.1$ and 0.33 are shown in figures 11(a, b) respectively; the same 2σ threshold was used in all three cases. Note that, even though the \tilde{u}_{r1} peak is used for trigger, the structure centre is not exactly coincident with the trigger location. In all three cases (figures 6 and 11 a, b), the structure centre occurs

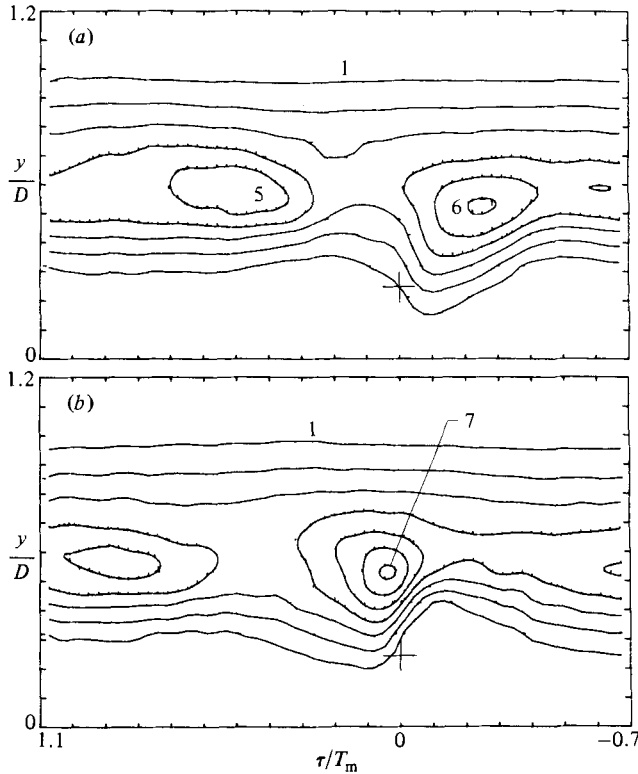


FIGURE 10. Ω_z/f_m contours educed by \tilde{v}_{r1} signal. Criteria used are (a) $\tilde{v}_{r1} < -2\sigma$, (b) $\tilde{v}_{r1} > 2\sigma$.

slightly to the right or at a slightly earlier time. In other words, the structure footprint lags the structure itself. For the preferred-mode structures induced under controlled excitation (see I), this was also the trend found upstream of $x/D = 3$, but the trend reversed downstream. This lag of the footprint occurs owing to the characteristic ‘tilt’ of the structure with respect to the jet axis; thus the farther is the sensor from the structure centre the more is this lag. In the present case, for $y/D = 0.1, 0.25$ and 0.33 , the structure centres occurred at $\tau = 0.1T_m, 0.08T_m$ and $0.04T_m$ respectively.

Note that, although the structure centre occurs closest to the trigger in figure 11 (b), the peak vorticity level is less than that in figure 6. This is because the reference probe in the former case is inside the shear layer ($U/U_e = 0.95$) and turbulent fluctuations in \tilde{u}_{r1} introduces spurious triggers and thus smear the educed structure. On the other hand, for $y/D = 0.1$, the structure centre is farther from the trigger in y as well as in τ and, as a result, the educed contours are also smeared out. Thus, while the reference probe needs to be as close to the structure as possible so that a sharp footprint is sensed, it should not be within the structure itself since small-scale fluctuations will then introduce smearing in the eduction. Note that, for the axial station under consideration ($x/D = 3$, a reference probe location of $y/D = 0.25$ (i.e. the $U/U_e \approx 0.99$ point) yields the best eduction.

3.2.3. Eduction with the zero-speed-side reference signal

The correlation between \tilde{u}_{r1} and \tilde{u}_{r2} and structure eduction with \tilde{u}_{r2} alone or with a joint criterion based on \tilde{u}_{r1} and \tilde{u}_{r2} are considered now. A large number of pairs

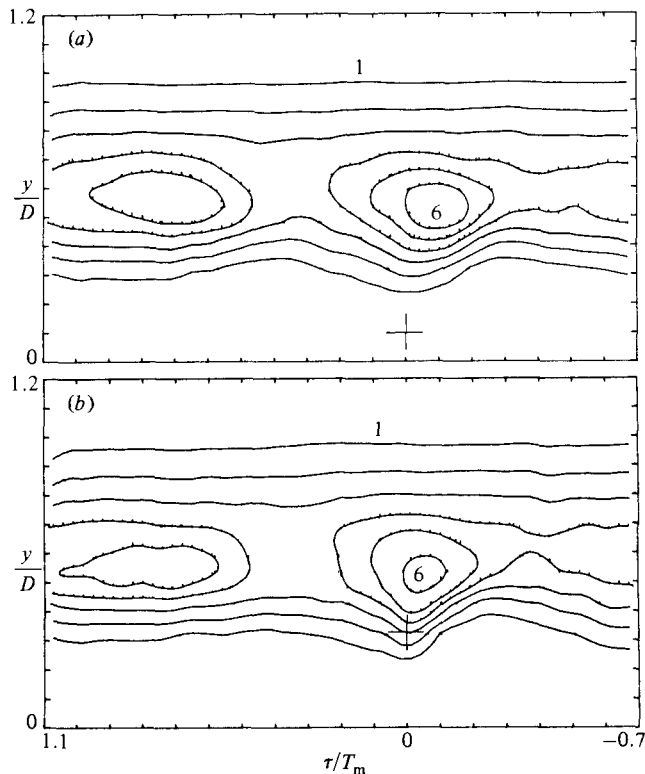


FIGURE 11. Ω_2/f_m contours educed by $\tilde{u}_{r1} > 2\sigma$ criterion with different transverse positions of the reference probe: (a) $y/D = 0.1$ ($U/U_e = 1.0$); (b) $y/D = 0.33$ ($U/U_e = 0.95$).

of \tilde{u}_{r1} and \tilde{u}_{r2} signals similar to the top pair in figure 4 were carefully scrutinized. Visual inspection showed that the positive peaks in \tilde{u}_{r2} and the negative peaks in \tilde{u}_{r1} possessed no apparent phase relationship.

The lack of correlation between the high-speed and zero-speed side signals is demonstrated in figure 12. It shows contours of (time-average) correlation coefficient R_{uu} between the u -signals from a fixed high-speed side probe and a measurement probe traversed in y . Large values of $R_{uu}(\tau, y)$ are encountered on the high-speed side, as to be expected, because the signals then are obtained from close-by locations. The alternate positive and negative regions of the contours on the high-speed side indicates the quasi-periodicity in the signal with a period T_m (see also figure 3a). Inside the mixing layer, the correlation coefficient is very low. On the zero-speed side, however, the contours reappear, but with very small values, indicating a faint 'footprint' of the large-scale structure. Recalling that spectra and autocorrelation of the velocity signals failed to reveal any periodicity on the zero-speed side (figures 2 and 3), while a clear periodicity was observed on the high-speed side, it is concluded that the best position for structure eduction with a single detection probe is the high-speed edge of the mixing layer.

Although visual inspection of the time traces revealed no phase relationship between the peaks of \tilde{u}_{r1} and \tilde{u}_{r2} , any possible hidden correlation was explored via a joint probability $p_{\frac{1}{2}}$ of the occurrence of a positive peak in \tilde{u}_{r2} relative to a negative peak in \tilde{u}_{r1} . The instants of occurrence of the negative peaks in \tilde{u}_{r1} below a threshold of -2σ were first detected. The simultaneous \tilde{u}_{r2} signal (time series) was then

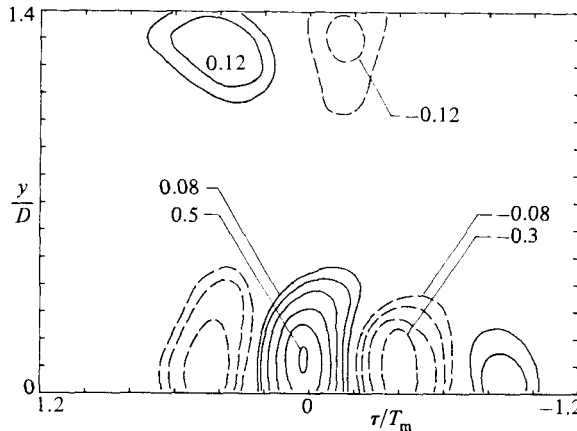


FIGURE 12. Correlation coefficient for \tilde{u}_{r1} and \tilde{u} -signal; \tilde{u}_{r1} from the $U/U_e \approx 0.99$ point ($y/D = 0.25$).

searched to find the instants of occurrences of positive peaks. This gave the joint probability $p_{\frac{1}{2}}$ as a function of the time delay with respect to the negative peaks in \tilde{u}_{r1} . A peak in $p_{\frac{1}{2}}(\tau)$ would indicate a predominant phase relationship between the positive peaks in \tilde{u}_{r2} and the negative peaks in \tilde{u}_{r1} . But, commensurate with the data in figure 12, $p_{\frac{1}{2}}(\tau)$ did not exhibit any identifiable peak (not shown), and the result was similar when all possible combinations of positive and negative peaks in \tilde{u}_{r1} and \tilde{u}_{r2} were considered.

These data thus indicate that, unlike in the plane shear layer at a low Reynolds number studied by Browand & Weidman (1976), conditional sampling triggered on a joint criterion based on \tilde{u}_{r1} and \tilde{u}_{r2} will not succeed in the present flow. Note that Browand & Weidman not only found definite phase relationships between the peaks of \tilde{u}_{r1} and \tilde{u}_{r2} but used different phase relationships to educe different stages of structure interaction. In the axisymmetric mixing layer, Yule (1978) had also failed to educe any structure by using a 'double-trigger' criterion. While discussing the contrast of Browand & Weidman's success, Yule conjectured that perhaps the plane-mixing-layer flow of Browand & Weidman corresponded to the early transitional flow in the circular jet. However, our investigation in a plane mixing layer shows that \tilde{u} -signals from the high- and low-speed sides are indeed well correlated even at large downstream distances where $Re_x \approx 2 \times 10^6$. We believe that the lack of correlation between \tilde{u}_{r1} and \tilde{u}_{r2} in the axisymmetric case can be traced to the flow geometry, which results in a dilated structure signature on the low-speed side. The axisymmetric configuration is also responsible for enhanced tearing and fractional pairing (Clark 1979). These, together with possible random occurrences of different mode structures (Moore 1977) should explain the loss of correlation across the axisymmetric mixing layer.

As expected, efforts to educe the structures with the zero-speed-side reference signal \tilde{u}_{r2} alone led to poor results. The Ω_z distributions educed by using the positive peaks of \tilde{u}_{r2} ($> 2\sigma$) are shown in figure 13; the reference probe position was $y/D = 1.25$ ($U/U_e \approx 0.01$). The educed vorticity field has some resemblance to that educed by the $\tilde{u}_{r1} < -2\sigma$ criterion (figure 5), but it is obvious that the structures obtained in figure 13 are smeared out. It is interesting to note, however, that the structure spacing is approximately the same as in figures 5 and 6. Thus the reference probe on the zero-speed side senses the 'footprint' of the same large-scale structure that produces a stronger

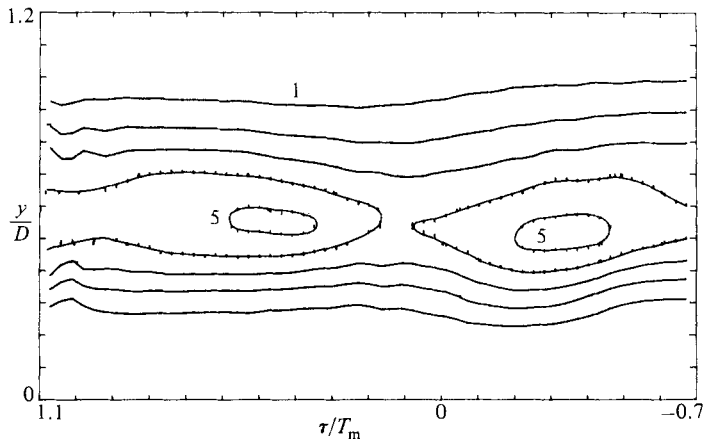


FIGURE 13. Ω_z/f_m contours educed by the $\tilde{u}_{r2} > 2\sigma$ criterion for reference probe at $y/D = 1.25$ ($U/U_e \approx 0.01$).

footprint on the high-speed side. This (once again) proves that Lau's (1979) 'two-street' model cannot be correct. Eduction based on the negative peaks in \tilde{u}_{r2} and for different positions of the reference probe on the zero-speed side (e.g. at the $U/U_e \approx 0.05$ point where \tilde{u}_{r2} shows large positive peaks) gave Ω_z contours which were even more smeared out than those in figure 13.

It is also noteworthy that eduction with $\tilde{u}_{r1} (> 2\sigma)$ but carried out on the (diametrically) opposite side of the axisymmetric mixing layer gave Ω_z contours similar to figure 6. These data (not shown for space conservation) exhibited increased smearing because the eduction was done in a region far away from the trigger probe, but, more importantly, the centre of the structure appeared at $\tau = 0$, as in figure 6. This would indicate that, even though higher-order instability modes may be occurring randomly, the present flow must be dominated by the axisymmetric mode, i.e. the ring-shaped structures.

3.2.4. Use of a joint probability of \tilde{u}_{r1} and \tilde{v}_{r1} for eduction

The peaks and troughs of the \tilde{u}_{r1} and \tilde{v}_{r1} signals from an X-wire reference probe placed on the high-speed side showed a definite phase relationship on the average. Thus a plot of the probability p_i of the occurrence of the negative peaks in \tilde{v}_{r1} relative to the positive peaks in \tilde{u}_{r1} , showed a definite peak at a certain phase difference. This is shown in figure 14 for $y/D = 0.25$, where the troughs of \tilde{v}_{r1} are found to lag the peaks of \tilde{u}_{r1} by about 40° . It was observed that this phase lag increases with increasing radial distance. The amplitude of the peak also depends on the transverse location, being a maximum at $y/D \approx 0.25$ ($U/U_e \approx 0.99$). The peak disappears on the jet axis and at transverse distances $y/D \lesssim 0.35$ ($U/U_e \lesssim 0.9$).

The phase relationship of \tilde{u}_{r1} and \tilde{v}_{r1} was utilized in an effort to improve the eduction. Ω_z contours were educed (not shown) by \tilde{u}_{r1} peaks ($> 2\sigma$) which were preceded by \tilde{v}_{r1} troughs at about 40° phase lead. This was essentially a further refinement of the triggering based on the \tilde{u}_{r1} peaks. (Note that this eduction is equivalent to using the instantaneous Reynolds-stress signal for the trigger.) However, comparison of this educed structure with that in figure 6 did not reveal any noticeable improvement in the eduction. It was concluded that the simple

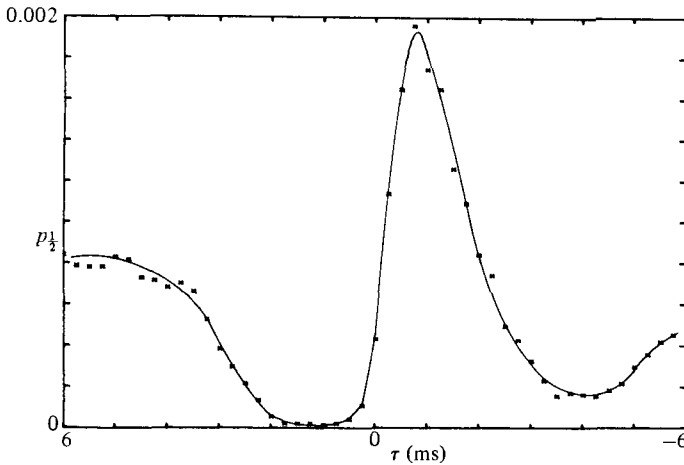


FIGURE 14. Joint probability function of the occurrence of \tilde{v}_{r1} trough relative to \tilde{u}_{r1} peak. Measurement at $y/D = 0.25$.

threshold criterion of $\tilde{u}_{r1} \gtrsim 2\sigma$ based on a single reference signal from the high-speed side ($U/U_e \approx 0.99$) was the optimum to capture the large-scale structures in the near field of the axisymmetric jet.

4. Structure characteristics and dependence on Reynolds number and initial condition

The optimum criterion of $\tilde{u}_{r1} > 2\sigma$ was then employed to educe the jet near-field coherent structure at $x/D = 3$ for different Reynolds numbers, initial conditions and amplitudes of excitation (at the preferred mode). The sensitivity of the structure to these three parameters is discussed. Ω_z is still used as the principal property for these comparative studies. The distributions of a few other properties characterizing the educed structure are briefly discussed in §4.3.

4.1. Effect of Re_D and initial condition

Figures 15(a, b, d) show the Ω_z contours for three different Re_D values of 5.5×10^4 , 3.3×10^5 and 8.0×10^5 respectively. While these three figures are for fully turbulent initial boundary layers, figure 15(c) shows Ω_z contours for the $Re_D = 3.3 \times 10^5$ jet with initially laminar boundary layer. The contour patterns in these figures are essentially similar to those in figure 6, which is for $Re_D = 1.1 \times 10^5$ with initially turbulent boundary layer. The educed structures do not show any noticeable dependence on Re_D . This demonstrates that the eduction criterion is successful even at the highest (available) Re_D and that any Re_D dependence, if present, is within the experimental uncertainty. Note that in I the peak vorticity was found to be the same at different Re_D , but the vorticity-contour shape and the coherent Reynolds stress magnitudes were found to be somewhat dependent on Re_D .

Comparison of figures 15(b, c), however, indicates some smearing of the educed structure for the initially laminar case. Similar was the conclusion from the contours of other structure properties at this Re_D as well as Ω_z contours at a few other Re_D values (not shown). This observation is consistent with flow-visualization experiments (Clark 1979), in which the structures appeared more disorganized in the initially

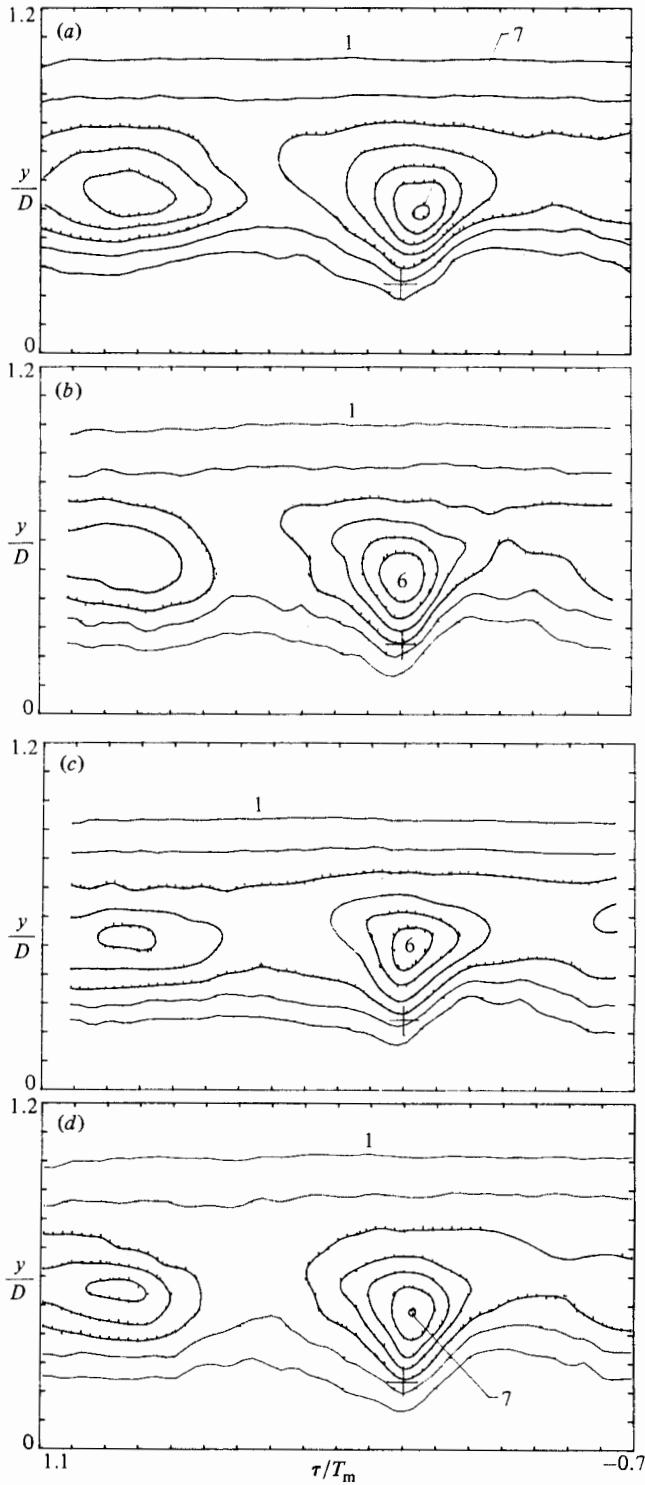


FIGURE 15. Ω_z/f_m contours for different jets. All measurements at $x/D = 3$. (L) for laminar and (T) for turbulent initial boundary layers. (a) $Re_D = 55000$ (T), 7.6 cm jet; (b) $Re_D = 330000$ (T), 27 cm jet; (c) $Re_D = 330000$ (L), 27 cm jet; (d) $Re_D = 800000$ (T), 27 cm jet.

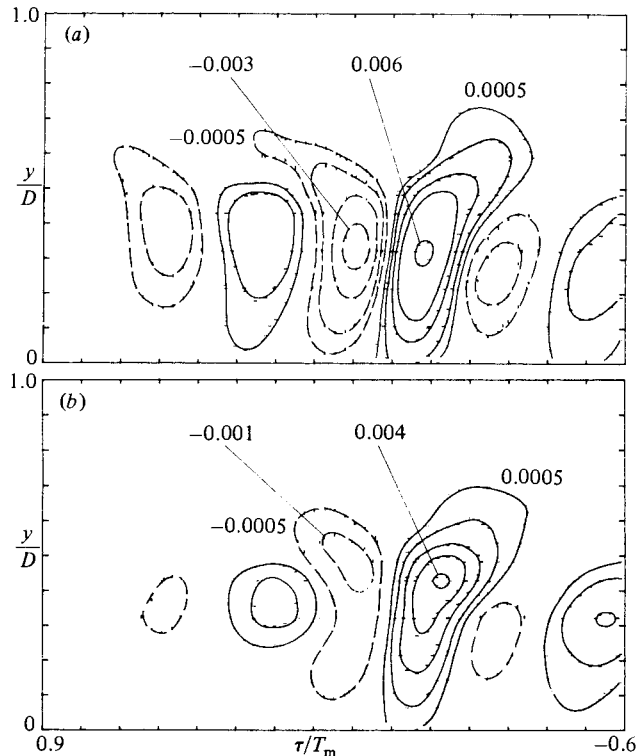


FIGURE 16. $\langle u_p v_p \rangle / U_c^2$ for $Re_D = 330000$; (a) turbulent; (b) laminar. Unmarked contour levels are: -0.002 , -0.001 , 0.001 , 0.002 , 0.003 .

laminar boundary-layer case as compared to the initially turbulent case. The stronger repeated structure for the turbulent cases also suggests that the structures occur more periodically in this flow. Note that this periodicity is evident at all Reynolds numbers.

The weaker structures in the laminar initial case is further demonstrated by the coherent Reynolds stress $\langle u_p v_p \rangle$, shown in figures 16(a, b) corresponding to the cases of figures 15(b, c) respectively. Note that $\langle u_p v_p \rangle$ shows regions of alternating positive and negative contributions. These distributions will be further discussed in §4.3, where these will be compared with those in an excited axisymmetric layer and an unexcited plane mixing layer. But consistent with the foregoing observations, the peak values and the transverse extents of $\langle u_p v_p \rangle$ are found to be larger for the initially turbulent case.

In the initially laminar boundary-layer case, the structures first roll up at a frequency f_s which scales on the initial shear-layer thickness (e.g. θ). These structures then antiscade to the jet preferred-mode frequency f_m , scaling on the jet diameter D . Since f_s corresponds to $St_\theta \approx 0.012$ and f_m (measured at $x = 3$)/ D to $St_D \approx 0.45$, the ratio between the two, i.e. $f_s/f_m \approx 0.027D/\theta$, controls the number of stages of pairing required to reach f_m from f_s . When pairing is involved, the triggering condition may capture structures in widely different stages of their development. Also, being a relatively violent process, a pairing stage may introduce some 'jitter' in the resulting structure detected downstream compared with the case where no pairing is involved. This jitter will increase with increasing number of pairings. Furthermore, if $f_s \gg f_m$, amalgamations may involve more than two structures and thus the detected structures would vary from one to another depending on how many

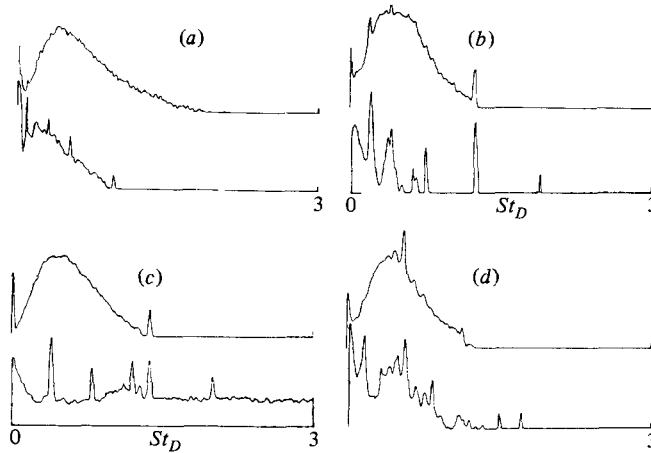


FIGURE 17. \tilde{u} -spectra on the axis of different jets: (a) $Re_D = 25000$, 2.54 cm jet; (b) $Re_D = 800000$, 27 cm jet; (c) $Re_D = 930000$, 30 cm jet; (d) $Re_D = 550000$, 15 cm jet. Turbulent initial boundary layer for all cases; in each case, lower trace for exit plane and upper trace for $x/D = 3$.

initially rolled-up structures actually merged. On the other hand, when the shear layer is initially turbulent, the structure roll-up occurs mostly at the frequency f_m and the structure persists without pairing. This should explain the observed differences between the educed structures in the initially laminar and initially turbulent cases.

\tilde{u} -spectra traces (figure 17) further demonstrate the Reynolds-number independence of the large-scale structure but a remarkable dependence on the background disturbance characteristics. Four pairs of the traces are shown for four cases (described in the figure caption) covering a Re_D range of 2.5×10^4 – 9.3×10^5 . The lower trace in each pair is for the exit plane and the upper one for $x/D = 3$, both on the axis of the jet. The (linear) abscissa range for all traces cover $0 \leq St_D \leq 3$. The (logarithmic) ordinate scale is the same for all upper traces; relative to this, the lower traces are magnified by 20 dB. The spectra at the exit are indicators of the background disturbance characteristics; note that in the magnified ordinate of these traces the spectral spikes at 60 Hz and harmonics, due to linearizer noise, appear prominently but are of no significance to the flow. Note also that the corresponding pair of traces for $Re_D = 110000$ have been included in figure 7. The upper traces for all the cases are characterized by a broadband hump with a modal frequency of $St_D \approx 0.45$. For a ‘clean’ initial condition as in figure 7 or for broadband background noise as in figures 17(a, c), the spectra traces at $x/D = 3$ are essentially identical, indicating similar characteristics of the large-scale structures. However, if the background disturbance contains a sharp peak, as in figure 17(d), which falls in the ‘sensitivity range’ of the jet, the large-scale structure formation locks onto this disturbance component and thus spectra at $x/D = 3$ also exhibit a largely amplified peak at the corresponding frequency. In such cases, the structure strength and organization can significantly depend on the amplitude of the disturbance component. This is demonstrated by the following data.

4.2. Effect of excitation amplitude on the structure

Figure 8 showed Ω_z contours at $Re_D = 110000$ with artificial excitation at $St_D = 0.49$ and $u'_{te}/U_e = 0.1\%$. The educed structures for the natural and the excitation cases were found to be quite similar. However, higher amplitudes of excitation can affect

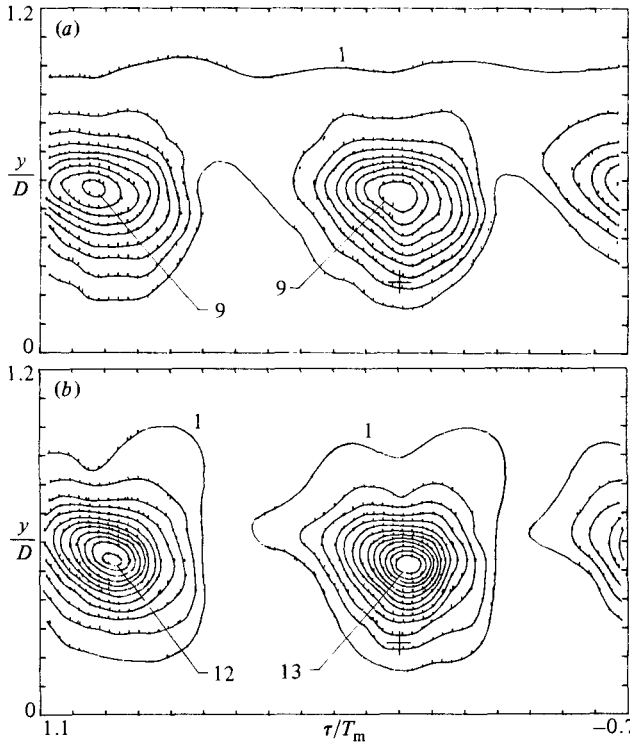


FIGURE 18. Ω_z/f_m contours for the excited flow of figure 7, but for excitation levels (a) $u'_{te}/U_e = 0.5\%$, (b) $u'_{te}/U_e = 1.5\%$.

the structures significantly. Figures 18(a, b) show Ω_z contours for (the same flow as in figure 8 but higher) excitation amplitudes of 0.5 and 1.5%, respectively. Since the excitation even at the level of 0.1% (figures 7 and 8) results in periodic passage of the structures, it is reasonable to believe that the differences in the structures in figures 18(a, b) are not caused by the dispersions in the structure properties alone. In particular, the large variation in the Ω_z peak value between figures 18(a, b) suggests that the structures are also modified (i.e. augmented or strengthened) besides being organized (i.e. made periodic) by the large-amplitude excitation. The explanation for this is unclear, but the following is plausible. Under excitation, the boundary layer at the point of separation is periodically thickened and thinned, producing a temporal variation of coherent vorticity which is shed into the resulting shear layer. The periodic distribution of vorticity lumps released into the shear layer will be accentuated at higher amplitudes of excitation, and thus the structure will continue to be controlled by the excitation amplitude. Note that, although the peak vorticity is higher for the higher amplitude, the estimated net circulation per period remains unchanged. This can be roughly inferred from inspection of the vorticity contours; the area enclosed by the outer contours shrinks from figure 18(a) to (b).

What would be the maximum excitation level for which this modification can be neglected? A clear answer to this question will require a prohibitive amount of data processing. But, based on the above data, it may be reasonable to assume that for excitation amplitudes u'_{te}/U_e less than 0.1%, the effect may be only an organization of the structures with negligible modification. As is apparent from figure 17,

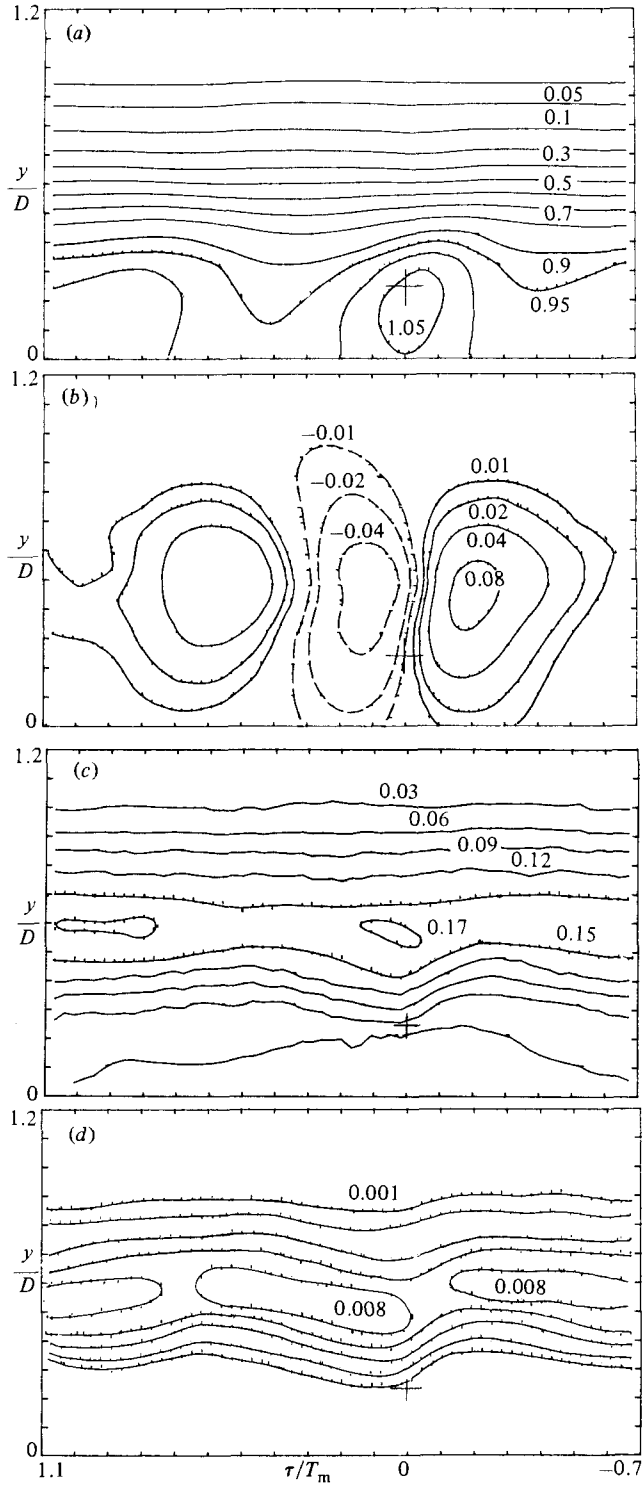


FIGURE 19. Coherent structure properties corresponding to the educed structure of figure 6:
 (a) $\langle u \rangle / U_e$; (b) $\langle v \rangle / U_e$; (c) $\langle u^2 \rangle^{1/2} / U_e$; (d) $\langle u_r v_r \rangle / U_e^2$.

large-amplitude disturbances of broad-band spectral distribution do not affect the structures downstream. But disturbances at isolated frequencies within the unstable band (e.g. as in figure 17*d*) can significantly modify the structures.

4.3. Other properties of the educed structure

For the natural structure at $Re_D = 110000$ in figure 6, a few other properties of interest are documented in figure 19. The $\langle u \rangle$ and $\langle v \rangle$ contours are shown in figures 19(*a, b*) respectively. These distributions are essentially similar to those for the axisymmetric mixing layer under excitation at the preferred mode (see I). Note that, even if the local time average were subtracted from $\langle u \rangle$, the corresponding contours will not resemble the structure boundary, a situation quite different from the boundary-layer 'spot'. The contours of $\langle v \rangle$ illustrate that the structure transports fluid radially outward at its front and radially inward at its back; the outward velocity is larger than (peak values are about twice) the inward velocity. The $\langle v \rangle$ distribution in this case is different from that in a plane mixing layer, where the outward and inward velocities are comparable; this is consistent with a faster spreading rate in the axisymmetric mixing layer.

The incoherent longitudinal fluctuation intensity and Reynolds stress are shown in figures 19(*c, d*) respectively. The $\langle u_r^2 \rangle^{\frac{1}{2}}$ distribution (figure 19*c*) is characterized by a peak coinciding with the structure centre. (Note that the + sign in these figures denotes the location of the trigger and not the structure centre.) However, the structure boundary is not clearly identified by $\langle u_r^2 \rangle^{\frac{1}{2}}$, and with increasing smearing away from the trigger the $\langle u_r^2 \rangle^{\frac{1}{2}}$ contours tend to coincide with the total time-average intensity (u') contours at either end of the timespan.

It is interesting to compare the Reynolds-stress distributions with those in the excited axisymmetric mixing layer and those in the natural plane mixing layer. The $\langle u_r v_r \rangle$ distribution in the present case agrees generally with those in both of the above cases. The structure centre coincides with the 'saddle point' of the $\langle u_r v_r \rangle$ distribution, as is to be expected (see I). However, the $\langle u_r v_r \rangle$ distributions in the excited axisymmetric mixing layer are more kinked around the saddle points, indicating more organized and strengthened structures. This is consistent with the results summarized in §4.2.

The $\langle u_p v_p \rangle$ contours, shown in figure 16, exhibit noticeable differences from the corresponding data in the excited axisymmetric mixing layer. The peak values of $\langle u_p v_p \rangle$ are much less compared to those in the excitation case. The orientations of the contour patterns are also somewhat different. However, the general distribution of these contours, having alternately positive and negative regions and occurring on the high-speed side, for the two cases agree fairly well. The 'cloverleaf'-type distribution of the $\langle u_p v_p \rangle$ contours for the natural structures in the plane mixing layer, on the other hand, is largely different. Furthermore, while the $\langle u_p v_p \rangle$ distribution in the plane mixing layer extended equally on the high- and the low-speed sides from the structure centres, significant $\langle u_p v_p \rangle$ occurs only on the high-speed side in the present case. The differences between structures in axisymmetric and plane mixing layers have been examined separately.

5. Concluding remarks

Eduction of the large-scale coherent structures in a turbulent shear flow suffers from the constraint that there is a large dispersion in the shape, size, orientation, strength, convection velocity, and passage times of these structures. This constraint had

prompted us and others to use controlled excitation, for the purpose of eduction, which paces the formation of structures at regular intervals and of equal strength. This approach minimizes dispersion as well as provides a phase reference for eduction. However, such an educed structure is interesting only if the flow has a 'preferred mode'. The axisymmetric jet does have a preferred-mode coherent structure (Crow & Champagne 1971; Zaman & Hussain 1980), which was organized by controlled excitation and studied previously by phase-averaging method. The question that remained unanswered was whether the structure in an unexcited axisymmetric jet could be educed and whether there was a simple but optimum conditional-sampling technique for educing the natural structure. It is shown in the foregoing that, by phase-locking onto the longitudinal velocity signal extrema, the natural coherent structure can be successfully educed.

Eduction triggered on the positive peaks in the \tilde{u} -signal (obtained from the high-speed side) is found to be more successful than when triggered on the negative peaks. This finding underscores the criticality of choosing a triggering criterion such that the trigger occurs as close to the structure centre as possible. The farther away is the structure centre from the trigger, the more is the smearing in the eduction due to progressive loss of phase-coherence. Thus, since the structure centre occurs closest to the positive peaks in \tilde{u}_{r1} but is time-shifted with respect to the negative peaks of \tilde{u}_{r1} , a better eduction is obtained when the former is used for trigger. Progressively higher threshold levels produced sharper contours of the structure properties. However, threshold levels higher than twice the standard deviation of the signal are not worth while as only marginal improvements are obtained while prohibitively increasing the experiment time. The optimum transverse location of the reference probe is found to be the high-speed edge of the mixing layer, say $U/U_e \approx 0.99$. Use of the $\tilde{v}(t)$ signal does not produce any improvement in the eduction, nor does a joint criterion based on both $\tilde{u}_r(t)$ and $\tilde{v}_r(t)$. Unlike in the plane mixing layer, the signals from the high- and low-speed sides of the axisymmetric layer are poorly correlated. Consequently, criteria based on two reference signals obtained from the two sides failed to educe the structures in the axisymmetric mixing layer. Tearing and fractional pairing, augmented by the axisymmetric configuration, appear to be responsible for a very weak signature of the structures on the low-speed side, allowing better eduction from the high-speed side only.

The simple eduction criterion of triggering on the positive peaks of \tilde{u}_{r1} ($> 2\sigma$), arrived at by the above considerations, was applied to axisymmetric mixing layers with different Reynolds numbers and initial conditions. The technique was successful in educing the structure at the highest available Re_D of 8×10^5 . No noticeable Re_D dependence of the natural large-scale structures was observed over the range $5 \times 10^4 < Re_D < 8 \times 10^5$; if there is any, this is within our experimental uncertainty. However, the structures, educed at $x/D = 3$, showed a mild but persistent dependence on the initial boundary-layer state. A relative disorganization of the structures (i.e. having larger dispersions in characteristic parameters) was observed when the initial boundary layer was laminar compared with the case when it was turbulent.

For the initially laminar shear layer, pairing of the initial structures introduces a 'jitter' in the detected structure, because detection 'captures' structures at different stages of their evolution after pairing. In contrast, the structures roll up and evolve at the preferred mode frequency in the initially turbulent case and thus the detected structure has less jitter, and the ensemble average suffers from less smearing.

Controlled excitation at the preferred mode can induce the large-scale coherent structures to become periodic even at small amplitudes (say $u'_{tc}/U_e = 0.1\%$), without

significant alteration from the natural structures. However, larger amplitudes of excitation can alter the structure details. With increasing amplitudes, the excitation results in progressively stronger structures, characterized by higher peak vorticity and coherent Reynolds stress.

This research was supported by the National Science Foundation under Grant ME-7822110.

REFERENCES

- ANTONIA, R. A., SATYAPRAKASH, B. R. & HUSSAIN, A. K. M. F. 1980 *Phys. Fluids* **23**, 695.
ARMSTRONG, R. R., MICHALKE, A. & FUCHS, H. V. 1977 *AIAA J.* **15**, 1011.
BRADSHAW, P. 1966 *J. Fluid Mech.* **26**, 225.
BROWAND, F. K. & LAUFER, J. 1975 *Turb. Liquids, Univ. Missouri-Rolla*, **5**, 333.
BROWAND, F. K. & WEIDMAN, P. D. 1976 *J. Fluid Mech.* **76**, 127.
BRUUN, H. H. 1977 *J. Fluid Mech.* **64**, 775.
BRUUN, H. H. 1979 *Proc. R. Soc. Lond. A* **367**, 193.
CLARK, A. R. 1979 Ph.D. thesis, Univ. Houston.
CROW, S. C. & CHAMPAGNE, F. H. 1971 *J. Fluid Mech.* **48**, 547.
DAVIES, P. O. A. L. & BAXTER, D. R. J. 1978 In *Structure and Mechanisms of Turbulence I* (ed. H. Fiedler). Lecture Notes in Physics, vol. 75, p. 125. Springer.
DRUBKA, R. E. & NAGIB, H. M. 1981 *IIT Fluid & Heat Transfer Rep.* R81-2.
HUSSAIN, A. K. M. F. & ZAMAN, K. B. M. Q. 1981 *J. Fluid Mech.* **110**, 39.
HUSSAIN, A. K. M. F. & ZEDAN, M. F. 1978 *Phys. Fluids* **21**, 1100.
KIBENS, V. 1980 *AIAA J.* **18**, 434.
KO, N. W. M. & DAVIES, P. O. A. L. 1971 *J. Fluid Mech.* **50**, 49.
LAU, J. C. 1979 *Proc. R. Soc. Lond. A* **368**, 547.
LAU, J. C., FISHER, M. J. & FUCHS, H. V. 1972 *J. Sound Vib.* **22**, 379.
MATTINGLY, G. E. & CHANG, C. C. 1974 *J. Fluid Mech.* **65**, 541.
MICHALKE, A. 1965 *J. Fluid Mech.* **23**, 521.
MOORE, C. J. 1977 *J. Fluid Mech.* **80**, 321.
PETERSEN, R. A. 1978 *J. Fluid Mech.* **89**, 469.
SOKOLOV, M., HUSSAIN, A. K. M. F., KLEIS, S. J. & HUSAIN, Z. D. 1980 *J. Fluid Mech.* **98**, 65.
WIDNALL, S. 1975 *Ann. Rev. Fluid Mech.* **7**, 141.
YULE, A. J. 1978 *J. Fluid Mech.* **89**, 413.
ZAMAN, K. B. M. Q. & HUSSAIN, A. K. M. F. 1980 *J. Fluid Mech.* **101**, 449.
ZAMAN, K. B. M. Q. & HUSSAIN, A. K. M. F. 1981 *J. Fluid Mech.* **112**, 379.
ZILBERMAN, M., WYGNANSKI, I. & KAPLAN, R. E. 1977 *Phys. Fluids Suppl.* **20**, S258.